THE UNIVERSITY *of* EDINBURGH

Edinburgh Research Explorer

Numerical investigation of nonlinear wave interaction with a submerged object

Citation for published version:
Ning, D, Li, Q & Viola, IM 2015, 'Numerical investigation of nonlinear wave interaction with a submerged object' Paper presented at 6th Conference on Computational Methods in Marine Engineering (Marine 2015) , Rome, Italy, 15/06/15 - 17/06/15, .

Link:
Link to publication record in Edinburgh Research Explorer

Document Version:
Early version, also known as pre-print

OPEN ACCESS

NUMERICAL INVESTIGATION OF NONLINEAR WAVE INTERACTION WITH A SUBMERGED OBJECT

DEZHI NING[*], QINGXIN LI[*] AND IGNAZIO MARIA VIOLA[†]

[*] State Key Laboratory of Coastal and Offshore Engineering
Dalian University of Technology
Dalian, 116024, China
e-mail: dzning@dlut.edu.cn, li_qing_xin@qq.com

[†] Institute for Energy Systems, School of Engineering
University of Edinburgh
Edinburgh, EH9 3JL, UK
email: i.m.viola@ed.ac.uk

Key words: Submerged object, nonlinear numerical wave flume, higher-order boundary element method, higher harmonics

Abstract. Submerged objects are widely occurred in ocean and coastal engineering. Their presence influences the neighbouring flow field and even generates higher harmonic waves. A two-dimensional fully nonlinear numerical wave flume, based on a time-domain higher-order boundary element method is developed to investigate nonlinear interactions between regular waves and a submerged object. The incident wave is generated by the inner-source wavemaker. Fully nonlinear kinematics and dynamics boundary conditions are satisfied on the transient free surface. A mixed Eulerian-Lagrangian technique combined with the fourth-order Runge-Kutta scheme is used as the time marching process. A four-point method is used to separate bound and free harmonic waves. The proposed model is verified against the experimental and other numerical data for nonlinear waves scattering by a submerged trapezoid and a submerged horizontal cylinder, respectively. Numerical tests are performed to investigate the effects of submergence and characterised length of a submerged object, static water depth on the high free harmonics.

1 INTRODUCTION

As an important breakwater-type structure, submerged objects have been commonly used to protect coastal community and infrastructure such as harbours and pipelines. It allows seawater to exchange freely between the sheltered region and the open sea, prevents stagnation and the transportation of sediment of the natural seabed. Compared with other types of breakwater, submerged objects can assure open scenic views and prevent high wave impact load on the breakwater structure. Wave propagation over an immersed obstacle has been widely investigated during the past decades. When waves propagate over a submerged object, there would be energy consumption, energy reflection and energy propagation. In the process of wave transformation, high bound and free harmonic waves are generated due to nonlinear shoaling effect, which may induce damage to the coastal structures and erosion of

the coastline. Therefore, it is of practical importance to consider the effects of submerged objects on wave transformation.

Numerous works have been performed on the physical mechanism of harmonics generation and the nonlinear interaction among these harmonics. By means of physical model, Massel (1983) observed that the fundamental mode wave transfers energy to its higher bound harmonics over a submerged step and then transmits it downstream as high free harmonics in deep water. Grue (1992) conducted experiments of nonlinear waves over a submerged obstacle and found that the high free harmonic waves are prominent downstream the obstacle. The author concluded that superharmonic wave amplitudes grow up to a saturation value with the increase of incoming wave amplitude. Up to 25% of the incoming energy flux may be transferred to shorter waves. The second and third harmonic free waves can be up to 60% of the fundamental wave downstream of the obstacle. Rambabu (2005) used a numerical model to study the transmission characteristics of a submerged breakwater. His study aimed to determine the effects of submergence, crest width and initial wave conditions on the transmission characteristics of submerged breakwater. The results indicate that there is an optimum width ratio of crest width and water depth and clear spacing for achieving minimum transmission. Brossard and Chagdali (2001) adopted a new method based on the Doppler shift generated by a moving probes and used it to discriminate the incident fundamental mode and the reflected fundamental mode. Their study showed that the transfer of energy from the fundamental mode to higher harmonics is very large in the cases of small submergence depth. Teng et al. (2010) performed a numerical simulation of the free high harmonics induced by a monochromatic wave propagating over a submerged bar. The study showed that in case of weakly nonlinear waves, the amplitude of the *n*-th free harmonic tends to increase in proportion to the *n*-th power of the incident wave amplitude. Shih (2013) conducted experiments with various combination of undulating breakwaters collocated with various wave conditions. Arash and Mahmoud (2013) numerically studied the interaction of waves and fixed dual submerged cylinders by using a fully nonlinear numerical wave tank with higher-order boundary element method. The results are in good agreement with the experiment data. This study indicates that the viscosity effect on the computation of vertical forces is negligible in comparison with its effect on horizontal forces. The mean horizontal forces on the cylinders are in opposite directions. Hence, two cylinders tend to decrease the gap distance. Also, the magnitude of mean horizontal and vertical forces significantly increases when the gap distance decreases. Ning et al. (2014) numerically investigated the higher harmonics induced by wave propagating over a submerged obstacle in the presence of uniform current. It was found that, compared to the one computed with zero current the peak value of non-dimensional second free harmonic amplitude is shifted upstream in an opposing current, and this shift increases with the current-free wave amplitude. It is vice versa in following current.

In this paper, previous studies are extended further investigating the influence of submergence, characterised length of submerged object and water depth on free harmonic amplitudes at the lee side of the object. A two-dimensional (2D) fully nonlinear numerical wave flume is developed based on potential theory and a mixed Eulerian−Lagrangian higher-order boundary element method (HOBEM). The incident waves are generated by the inner sources in order to avoid reflections. A four-point method is used to separate free and bound harmonics at the same frequency. The proposed model is verified against experimental and

other numerical data for nonlinear waves scattering by a submerged trapezoid and a submerged horizontal cylinder, respectively.

The rest of the paper is structured as follow: in Section 2 the proposed numerical model is presented; in Section 3 the present model is verified against the available data; in Section 4 the results of high free harmonics amplitude induced by a submerged horizontal cylinder are presented and discussed; and conclusions are given in Section 5.

2 MATHEMATICAL FORMULATIONS

A monochromic wave propagation and transformation over a submerged obstacle in a 2D wave flume is considered (Figure 1). A Cartesian coordinate system $O(xz)$ is employed with its origin located at the still water level and the z-axis being positive upward. Let h denote the static water depth, h_s the submergence (i.e., the distance from the uppermost point of the body to the still water surface), t the time and η the free surface elevation above the still water level. Two damping layers are deployed at both ends of wave flume to dissipate the transmitted and reflected waves, respectively. Assuming the fluid inviscid and incompressible, and the flow irrotational, potential flow theory can be used inside the fluid domain Ω and the fluid velocity is described as the gradient of the velocity potential. The waves are generated by controlling the volume flux density of a vertical source distribution inside the model boundary.
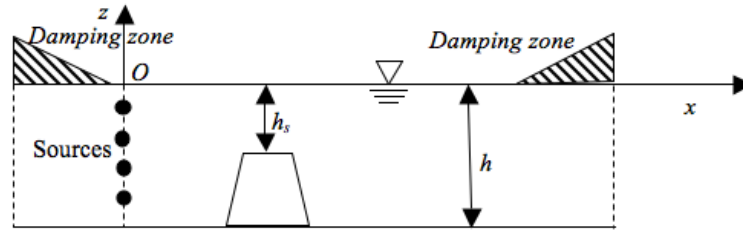

Figure 1: Schematic diagram of the numerical wave flume

The governing equation is the Poisson equation:

$$\nabla^2\phi = q^*(x_s,z,t) \tag{1}$$

where $q^*(x_s, z, t)$ is the pulsating volume flux density of the internal source distribution described as follow (Brorsen and Larsen, 1986):

$$q^*(x_s, z, t)=2V\delta(x-x_s) \tag{2}$$

where V is the horizontal flow speed; x_s is the horizontal position of the vertical source, and $\delta(x-x_s)$ is the Dirac delta function. In the present study, the horizontal velocity V is given as Stokes second-order analytical solution.

The fully nonlinear kinematic and dynamic boundary conditions are satisfied on the transient free surface. The mixed Eulerian-Lagrangian scheme is adopted to describe the time-dependent free surface with moving nodes. A damping layer with coefficient μ at the two ends

of the flume is added to gradually absorb the reflected and transmitted waves. Thus the free surface boundary conditions can be given as follow:

$$\begin{cases} \frac{dX(x,z)}{dt} = \nabla\phi - \mu(x)(X - X_0) \\ \frac{d\phi}{dt} = -g\eta + \frac{1}{2}|\nabla\phi|^2 - \mu(x)\phi \end{cases} \tag{3}$$

The damping coefficient $\mu(x)$ is defined as follow:

$$\mu(x) = \begin{cases} \omega(\dfrac{x - x_{1(2)}}{L_b})^2 & (x < x_1 \ or \ x > x_2) \\ 0 & otherwise \end{cases} \tag{4}$$

where x_1 and x_2 are the entrance positions of two damping zones, respectively; L_b is the length of the damping zone; the angular frequency ω and the wave number k satisfy the linear dispersive relation.

The boundaries at the bottom and the submerged object are considered impermeable and, thus, the zero normal velocity condition is imposed. Initial calm conditions are used.

By applying the Green's second identity, the above boundary value problem can be converted into the following boundary integral equation:

$$\alpha(p)\phi(p) = \int\limits_{\Gamma}(\phi(p)\frac{\partial G(p,q)}{\partial n} - G(p,q)\frac{\partial \phi(p)}{\partial n})\mathrm{d}\Gamma + \int\limits_{\Omega}q^*G(p,q)\mathrm{d}\Omega \tag{5}$$

where Γ represents the entire computational boundary; p and q are the source point (x_0, z_0) and the field point (x, z), respectively; and α is the solid angle coefficient. $G(p, q)$ is the Green function and can be written as $G(p, q)=\ln r/2\pi$, where $r = \sqrt{(x - x_0)^2 + (z - z_0)^2}$.

The above boundary integral equation for $(\phi, \partial\phi/\partial n)$ is solved by a boundary element method using a set of collocation nodes on the boundary and higher-order elements are used to interpolate among collocation points (three-node line elements are used to discretise the entire curved boundary surface). Both the boundary geometry and the physical variables are interpolated based on the nodal values and the quadratic shape functions within the boundary elements, thus the elements are isoparametric. The final algebraic system is assembled by moving the unknowns to the left-hand side of Eq. (5) and keeping the specified terms on the right-hand side.

As the discretised integral equation is always variant in time, all the boundary surfaces are re-gridded and updated at each time step. For the sake of better stability and convergence, the fourth-order Runga-Kutta scheme is used to predict the new variables (ϕ, x and η) at the next time-step. As the HOBEM is adopted, the derivatives of the velocity potential contained in the free-surface boundary conditions can be obtained by making use of the shape functions (see Ning et al., 2009, for details).

During the process of wave propagation over a submerged object, higher harmonic waves

will be induced due to nonlinear wave-wave interactions, which would start to be released as free waves when they enter the deep water at leeward. The surface elevation at a point x downstream the obstacle can be expressed as:

$$
\begin{aligned}
\eta(x,t) = {} & A_T^{(1)} \cos(kx - \omega t + \varphi_T^{(1)}) + A_R^{(1)} \cos(kx + \omega t + \varphi_R^{(1)}) \\
& + \sum_{n \geq 2}^{\infty} A_{TB}^{(n)} \cos[n(kx - \omega t) + \varphi_{TB}^{(n)}] + \sum_{n \geq 2}^{\infty} A_{RB}^{(n)} \cos[n(kx + \omega t) + \varphi_{RB}^{(n)}] \\
& + \sum_{n \geq 2}^{\infty} A_{TF}^{(n)} \cos[(k^{(n)}x - n\omega t) + \varphi_{TF}^{(n)}] + \sum_{n \geq 2}^{\infty} A_{RF}^{(n)} \cos[(k^{(n)}x + n\omega t) + \varphi_{RF}^{(n)}]
\end{aligned}
\tag{6}
$$

where A is the amplitude and the subscripts TB and TF, RB and RF denote transmitted bound and free waves, and reflected bound and free waves, respectively; the superscript n denotes the n-th harmonics; $k^{(n)}$ is the n-th ($n>2$) free wave numbers; $k^{(n)}$ and $n\omega$ satisfy the linear dispersive relation; and φ is the phase. In the present study, a four-point method developed by Ning et al. (2014) is used to solve Eq. (6) for separating bound and free higher harmonic waves and checking the efficiency of damping layer.

3   MODEL VALIDATIONS

In this section, the proposed numerical wave flume was validated by comparison with published experimental and numerical results of surface elevations for monochromatic wave propagation over a submerged trapezoidal bar, and experimental results of high free harmonic amplitudes induced by a submerged horizontal cylinder.

3.1 Monochromatic wave propagation over a submerged trapezoidal bar

To validate the present model, the developed numerical wave flume was firstly used to investigate the experimental example of monochromatic wave propagation over a submerged trapezoidal bar described by Beji and Battjes (1993) and Luth et al. (1994). In the experiment, the static water depth is h=0.4 m, the submerged depth h_s=0.3 m, the breadths of the top side and bottom side of the bar are 2.0 m and 11.0 m, respectively. The distance between the initial wave maker and the toe of the seaward side is 6.0 m. In the present numerical simulation, parameters for wave period T=2.02 s and wave amplitude A=0.01 m are used. The immerged sources are locate at x=0. The corresponding computational domain is 10.5λ long (where λ=2π/k denotes wave length) and, based on convergent numerical tests, it was chosen to use 210×6 cells in the horizontal and vertical directions, respectively. Two damping layers of 1.5λ in length are used at the ends of flume. The numerical step is chosen as Δt=T/60 and the total simulating time is 20T.
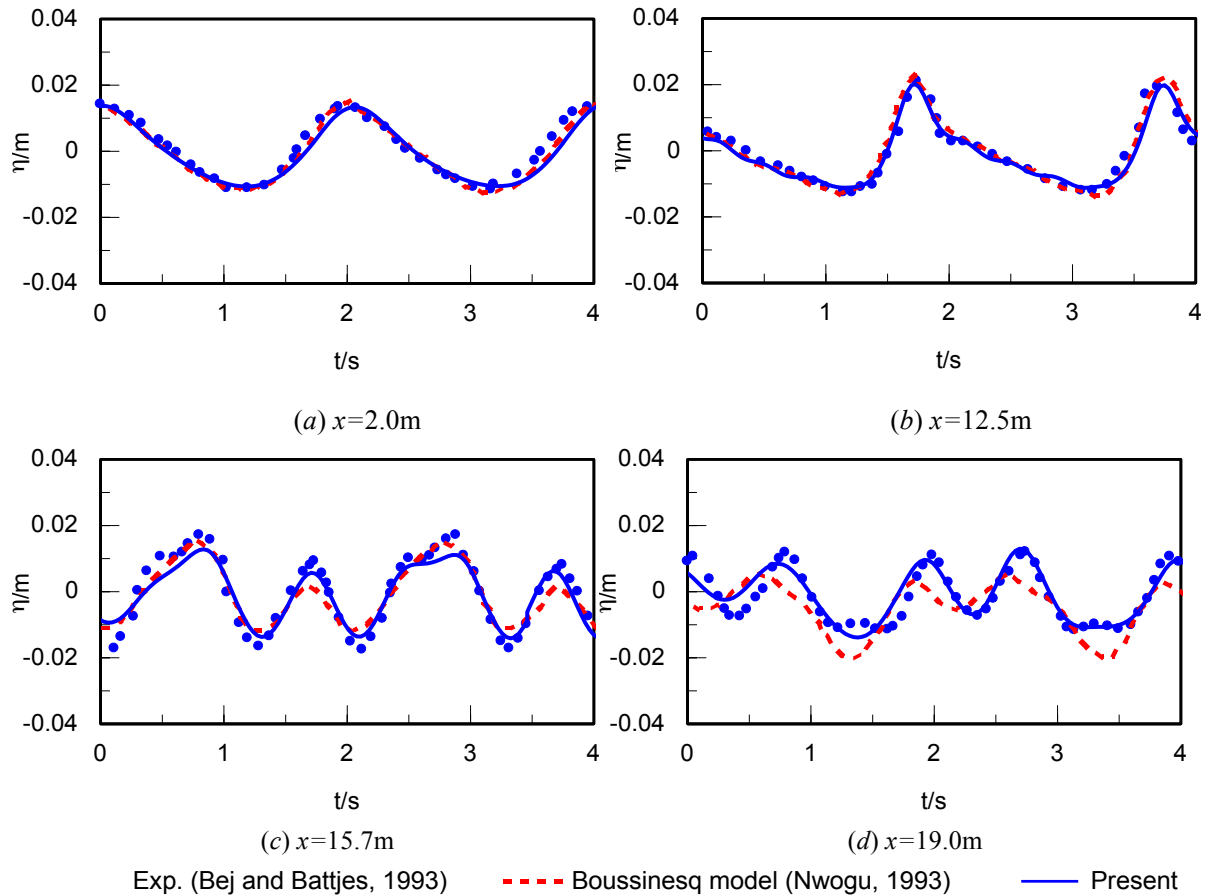
Figure 2 shows a snapshots of the wave profiles at t=18T and 20T. The vertical dash lines denote the end points of the top side, and the vertical solid lines represent the end points of the bottom side of the submerged bar. There is a good agreement between the solutions at these two instants, indicating numerical convergence. It is also found that while the wave profiles at the weather side of the submerged object are still regular and periodic, they are skewed at the lee side. This result is consistent with the findings of Peng et al. (2009) on the

transformation of wave asymmetries over a low-crested breakwater. It suggests that a number of harmonic wave components are generated at the lee side due to wave-wave nonlinear interaction. Additionally, the damping scheme at the ends of the numerical flume is effective, since most of the transmitted wave energy has been dissipated.
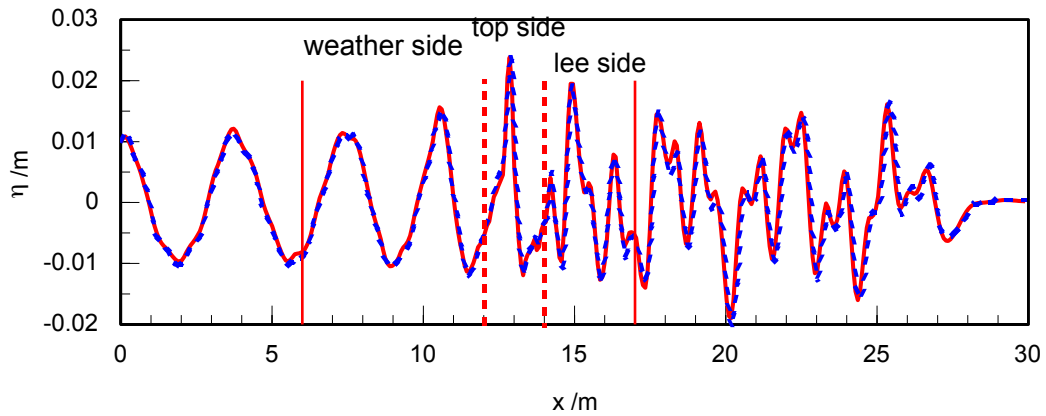
Figure 2: Distribution of wave elevation along the flume at t=18T and 20T (solid line:18T, dashed line: 20T)

Figure 3 gives the time series of wave elevations at specific points (x=2.0 m, 12.5 m, 15.7 m and 19.0 m) and comparisons among the present results, experimental data and the solutions of the extended Boussinesq model of Nwogu (1993). While there is a general good agreement between the three methods, for the points x=15.7 m and 19.0 m (i.e. the top and lee sides) the present model is in better agreement with the experimental data than the Boussinesq model. Afore the submerged bar, the wave profiles are symmetric and periodic, and wave nonlinearity is not apparent. However, the wave nonlinearity increases due to shallow water when waves reach the bar, and this results in wave power transformed from low-frequency component to high-frequency component. Thus high bound harmonics with the same propagation speed of the fundamental wave are generated. After the submerged bar, the asymmetry of wave profile is increased due to the decreased wave nonlinearity and high bound harmonics released as free harmonics with the increase of wave depth. Different phases of different free harmonics lead to the skewed wave profiles as shown in Figure 3(d).

(a) x=2.0m

(b) x=12.5m

(c) x=15.7m

(d) x=19.0m

Exp. (Bej and Battjes, 1993)   ▬ ▬ ▬ Boussinesq model (Nwogu, 1993)   ▬▬ Present

Figure 3: Time series of wave elevation measured experimentally and computed with a Boussinesq (Nwogu, 1993) and the present model

3.2 High free harmonics induced by a submerged horizontal cylinder

To test the ability of the four-point method to separate free and bound harmonics in waves, the experimental case for monochromic wave propagating over a submerged horizontal cylinder in quiescent water described by Grue (1992) is considered. The following parameters are chosen: static water depth h=0.45 m; cylinder radius R=0.1 m and 0.19 m; submerged depth h_s=0.05 m; wave period T=0.95 s and 0.82. Free surfaces in three stable wave periods are chosen to separate bound and free harmonics.

Figure 4 shows the distribution of high free harmonic wave amplitudes ($A_F^{(n)}/A$) with the incident wave amplitude A and comparison between the present numerical results and experimental data (Grue, 1992). The lines illustrate the present numerical results and the symbols illustrate the experimental data. The predicted fundamental and second-harmonic free wave amplitudes compare well with experiments for a range of incident wave amplitude. Initially, the fundamental wave amplitude is similar to the incident wave amplitude and then decreases with the increase of A, while the normalised second free harmonic amplitude

7

increases with the incident wave amplitude almost linearly, and then reaches a maximum value at a certain value of the incident amplitude. The second bound harmonic wave amplitude is much smaller than the second free harmonic wave and it is not shown here. Based on the four-point method, the amplitude of the reflected fundamental wave downstream of the structure results less than 5%, which is an index of the effectiveness of the damping zone.

(a) R=0.1m, h_s =0.05m, T=0.95 s

(b) R=0.1m, h_s=0.05 m, T=0.82 s

(c) R=0.19m, h_s=0.05 m, T=0.95 s
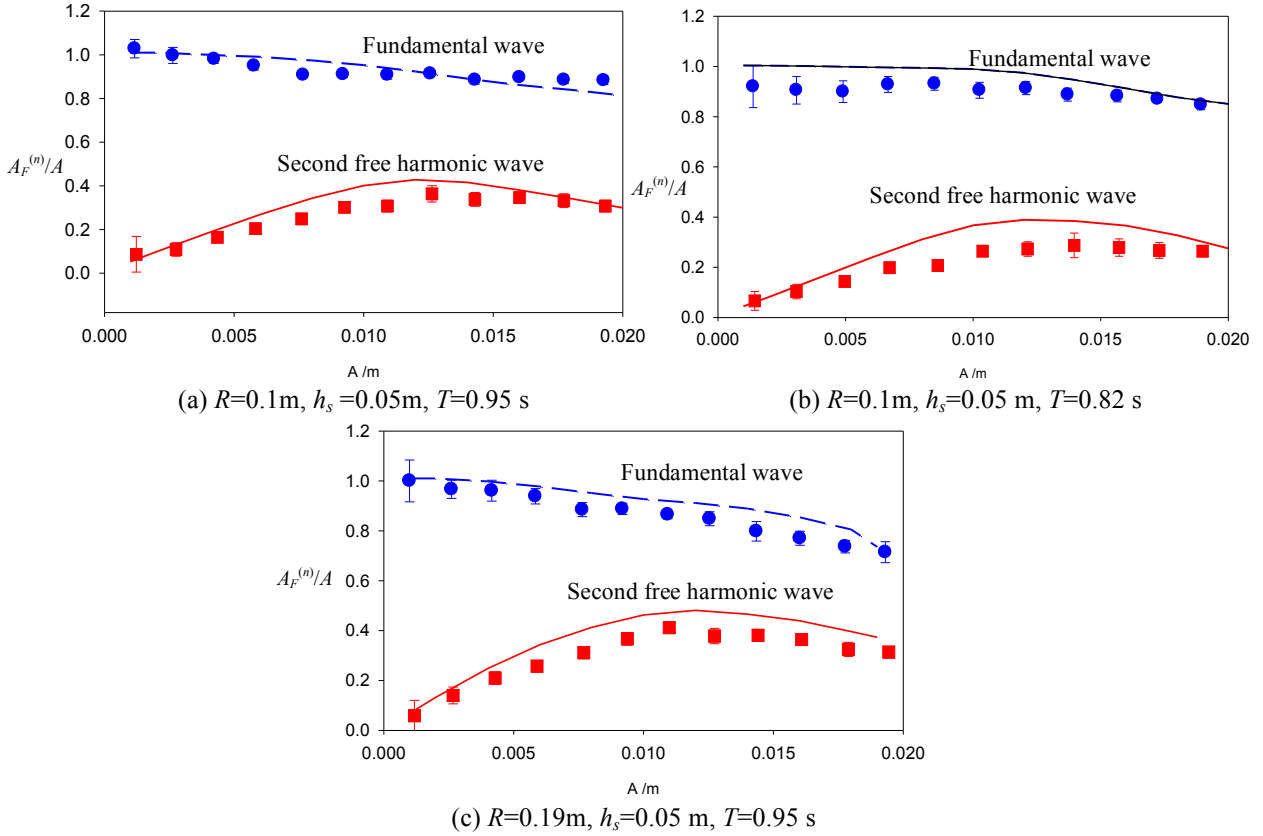
Figure 4: Comparisons of the normalised fundamental and second free harmonic amplitudes computed with the present numerical model (lines) and measured by Grue, 1992 (solid markers)

4   NUMERICAL RESULTS AND DISCUSSION

In this section, the proposed numerical model is applied to simulate wave propagating over a submerged horizontal cylinder and to study the induced high free harmonics. With the same conditions as in Subsection 3.2, the effects of submerged depth, characterised length and static water depth on high free harmonic amplitude are investigated.

4.1 Effect of submerged depth on high free harmonics

Figure 5 shows the distribution of dimensionless fundamental wave, second and third free harmonic wave amplitude with incident wave amplitude for three different submerged depths at the static water depth of h=0.45 m, cylinder radius R=0.1 m and wave period T=0.82 s. It

can be observed that the fundamental wave amplitude is close to the incident wave amplitude for the largest submergence (h_s=0.1 m) but, with the decrease of submergence h_s, it decreases with the incident amplitude. Conversely, both second and third free harmonic amplitudes increase with the decrease of submergence h_s. This phenomenon is due to the shallower water depth above the submerged object resulting in the stronger wave nonlinearity for the smaller submergence. Figure 5 (b) shows the second free harmonic amplitude, which firstly increases to a maximum up to the critical incident amplitude A_c, and then decreases with the increase of incident amplitude A. The critical incident amplitude A_c decreases with the increase of submergence h_s. However, in Figure 5 (c) there is not such a critical incident amplitude A_c, suggesting that there are more fundamental and second harmonics energy transferred to the third one at large-amplitude zone.

(a) Fundamental wave

(b) Second free harmonic wave

(c) Third free harmonic wave
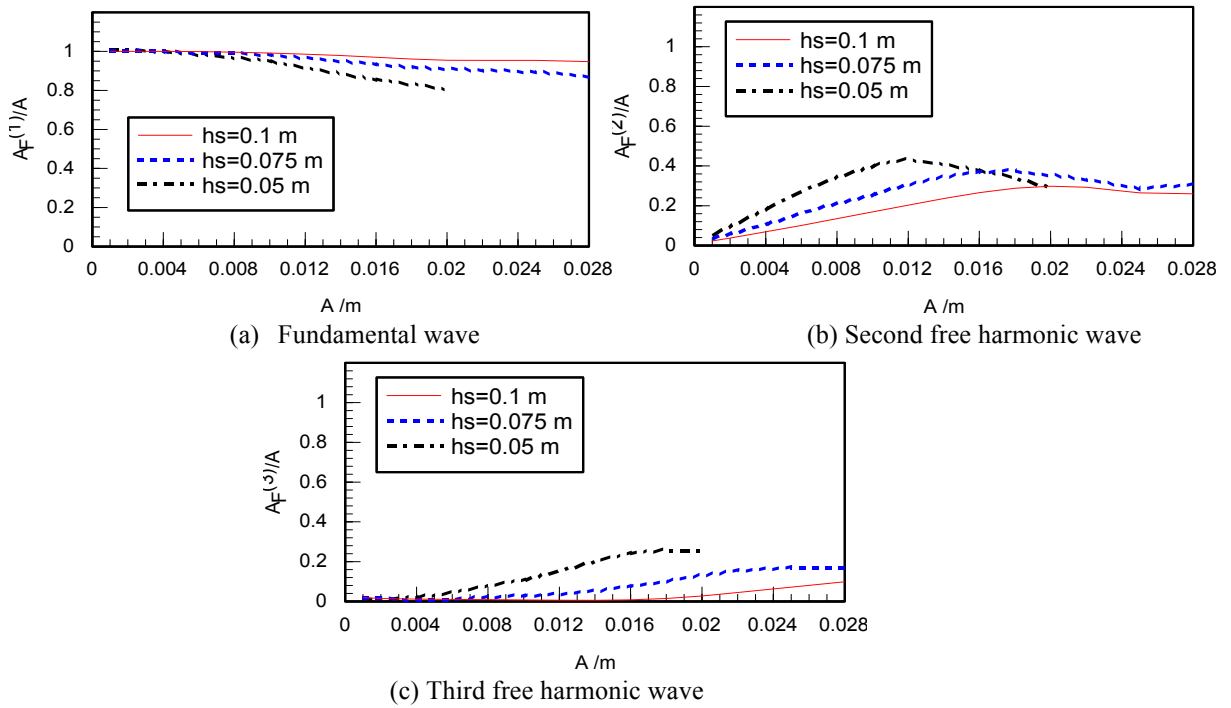
Figure 5: Distribution of normalised high free harmonic wave amplitude with incident wave amplitude for different submerged depths at h=0.45 m, R=0.1 m and T=0.82 s

## 4.2 Effect of characterised length on high free harmonics

By taking L=2R as the characterised length of the submerged object, Figure 6 shows the effect of the characterised length on high free harmonic wave amplitudes, where h=0.45 m, hs=0.075 m, T=0.82 s and three different cylinder radii R are considered. The fundamental wave amplitude decreases with the incident wave amplitude A and the negative slope is steeper for larger cylinder radii. Both second and third free harmonic wave amplitudes increase with the increase of the characterised length, which is similar to the cases of small submergence in Figure 5 (b) and (c). As the cylinder radius increases, the shallow water region above the object is lengthened, which induces more strong nonlinear waves released as high free harmonics in the deep water region at the lee side of the submerged object.

9

(a) Fundamental wave

(b) Second free harmonic wave

(c) Third free harmonic wave
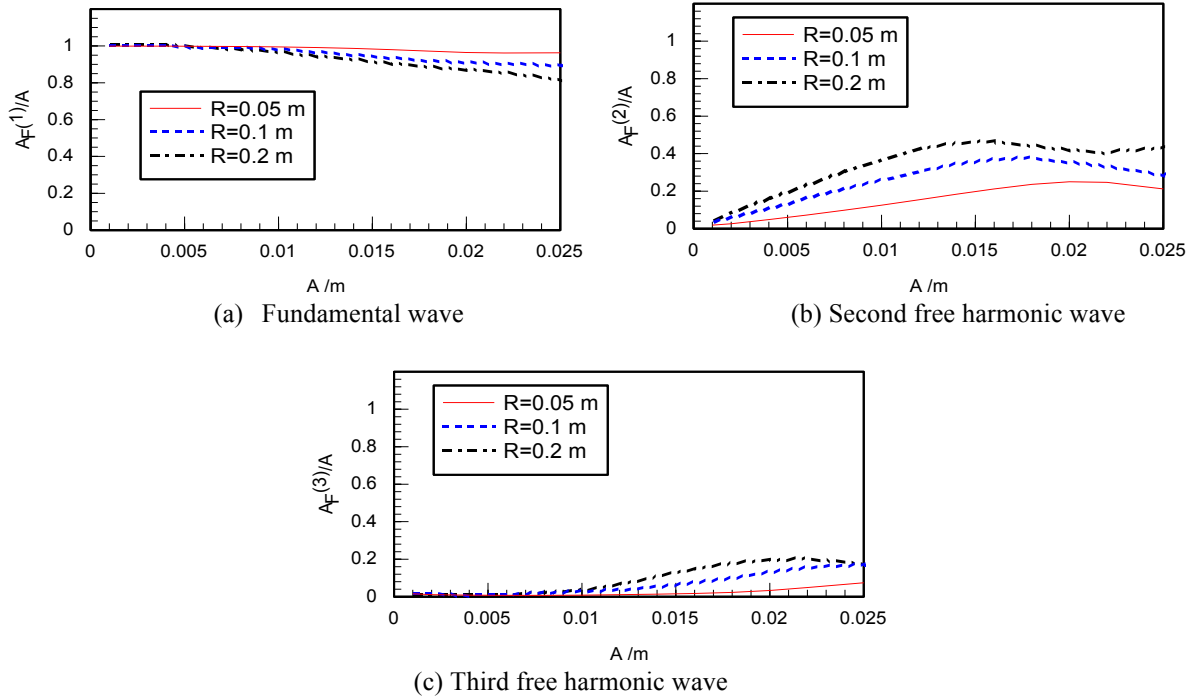
Figure 6: Distribution of normalised high free harmonic wave amplitude with incident wave amplitude for different radii

4.3 Effect of water depth on high free harmonics

Figure 7 presents the distribution of normalised fundamental wave, second and third free harmonic wave amplitudes with incident wave amplitude for three different water depth h at R=0.1 m, h_s=0.075 m and T=0.82 s. Little influence on the fundamental waves from water depth is observed. The same conclusion for second and third free harmonics in the small-incident-wave-amplitude zone can be drawn. When the water depth increases to a certain value, its influence on the free harmonics can be neglected. However, for the shallower water depth, the wave nonlinearity is enhanced. Variation of second and third free harmonic amplitudes is quite different from those in deeper water. The maximum second and third free harmonic amplitudes reach about 0.46 and 0.2 times incident wave amplitude A.

(a) Fundamental wave

(b) Second free harmonic wave

(c) Third free harmonic wave
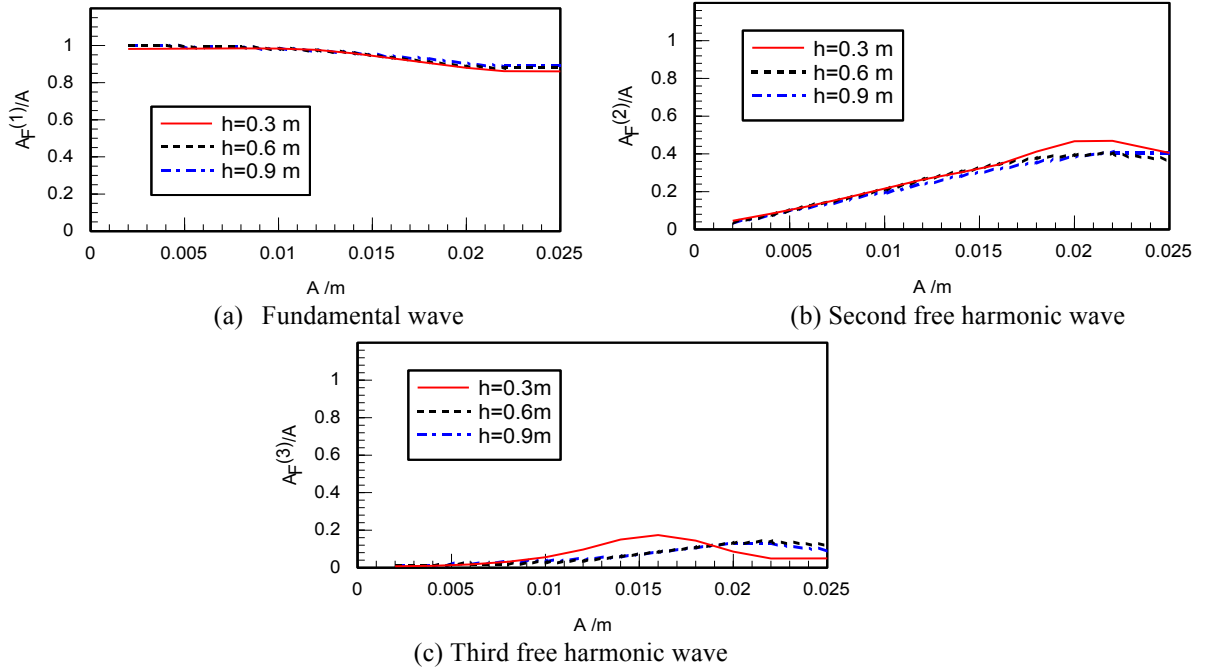
Figure 7: Distribution of normalised high free harmonic wave amplitude with incident wave amplitude for different water depths

5   CONCLUSIONS

A time-domain numerical model is implemented to model the interaction of monochromatic waves and a submerged object in a 2D wave flume. The proposed numerical model is based on potential theory and a higher-order boundary element method with a mixed Eulerian-Lagrangian approach to update the instantaneous free surface. By application of the 4th-order Runge-Kutta technique, the temporal update of the transient free surface was obtained from the fully nonlinear kinematic and dynamic free-surface boundary conditions. A four-point method is adopted to separate bound and free harmonics in the transmitted waves. The model is verified by comparing with both numerical and experimental published data. The influence of submerged depth, characterised length of the object and static water depth on high free harmonics are thereby investigated. The results show that the fundamental wave amplitude decreases and second and third free harmonic amplitudes increase by reducing the submergence or increasing the characterised length. There is a critical incident wave amplitude A_C at which second free harmonic amplitude reaches the maximum. With the decrease of submergence or increase of the characterised length, the critical amplitude A_C decreases, suggesting that a smaller incident wave amplitude A can lead to a stronger wave nonlinearity in the shallower water region. Water depth h shows less influence on fundamental wave amplitude and has no influence on second and third free harmonic amplitudes when water depth increases over a threshold.

11

ACKNOLEDGEMENTS

REFERENCES

[1] Abbasnia, A., and Ghiasi, M. Simulation of nonlinear wave interaction with dual cylinders in numerical wave tank. *Transactions of FAMENA* (2013). XXXVII-1

[2] Brorsen, M. and Larsen, J. Source generation of nonlinear gravity waves with the boundary integral equation method. *Coastal Engineering* (1987), **11**: 93-113.

[3] Brossard J. Experimental investigation of the harmonic generation by waves over a submerged plate. *Coastal Engineering*. (2001), **42**:277-290.

[4] Beji, S. and Battjes, J.A. Experimental investigations of wave propagation over a bar. *Coastal Engineering* (1993), **19**: 151-162.

[5] Grue, J. Nonlinear water waves at a submerged obstacle or bottom topography. *Journal of Fluid Mechanics* (1992), **244**:455-476.

[6] Luth, H.R., Klopman, G. and Kitou, N. Kinematics of waves breaking partially on an offshore bar; LDV measurements of waves with and without a net onshore current. Report H-1573, Delft Hydraulics (1994).

[7] Massel, S.R. Harmonic generation by waves propagating over a submerged step. *Coastal Engineering*. (1983), **7(4)**:357-380.

[8] Ning, D.Z., Teng, B., Zang, J. and Liu, S.X. An efficient model for transient surface waves in both finite and infinite water depths. *China Ocean Engineering* (2009), **23**:459-472.

[9] Ning, D.Z., Lin, H.X., Teng B. and Zou, Q.P. Higher harmonics induced by waves propagating over a submerged obstacle in the presence of uniform current. *China Ocean Engineering* (2014), **28**:725-738.

[10] Nwogu, O. An alternative form of the Boussinesq equations for nearshore wave propagation. *Journal of Waterway, Port, Coastal, and Ocean Engineering* (1993), **119**: 618–638.

[11] Peng, Z., Zou, Q.P., Reeve, D.E. and Wang, B. Parameterisation and transformation of wave asymmetries over a low crested breakwater. *Coastal Engineering* (2009), **56**(11-12):1123-1132.

[12] Rambabu, A.C., and Mani, J.S. Numerical prediction of performance of submerged breakwaters. *Ocean Engineering* (2005), **32(10)**:1235-1246.

[13] Shih, R.S,, Weng, W.K., Chou, C.R. Experimental determination on the reflectance characteristics of undulating submerged obstacle: comparison between regular and irregular wave response. *In the proceedings of the 23rd International Society of Offshore and Polar Engineers*, 30 June - 4 July, Anchorage, Alaska, US (2013).

[14] Teng, B.,Chen, L.,Ning, D.z. and Bai, W. Study on the higher harmonic waves over a submerged bar. *In the proceedings of the 25th International Workshop on Water Waves and Floating Bodies*, 9-12 May, Harbin, China (2010).